Article

Discovery Medicine 2026; 38(204): 229–242
https://doi.org/10.24976/Discov.Med.202638204.18

RSPO2 Accelerates Tendon-Bone Healing After Anterior Cruciate Ligament Reconstruction by Enhancing BMSCs-Induced M2 Macrophage Polarization

Chengbo Wu[1], Yong Yang[2,*]

[1]Trauma Orthopaedics, Yantaishan Hospital, 264001 Yantai, Shandong, China
[2]Department of Sports Medicine, Yantaishan Hospital, 264001 Yantai, Shandong, China
*Correspondence: 15553565976@163.com (Yong Yang)
Submitted: 21 November 2025 Revised: 18 December 2025 Accepted: 26 December 2025 Published: 20 January 2026

Background: Tendon–bone healing after anterior cruciate ligament reconstruction (ACLR) remains limited by insufficient bone formation and an unfavorable inflammatory microenvironment. Although bone marrow–derived mesenchymal stem cells (BMSCs) have therapeutic potential, their osteogenic and immunomodulatory effects are suboptimal. Additionally, the role of R-spondin 2 (RSPO2) in enhancing BMSC-mediated tendon–bone healing remains unclear. This study aims to investigate the role of RSPO2 in promoting the osteogenic differentiation of BMSCs and its effect on M2 macrophage polarization, as well as the potential of RSPO2 combined with BMSCs to accelerate tendon-bone healing after ACLR.

Methods: During the osteogenic induction of BMSCs, low, medium, and high concentrations of RSPO2 recombinant protein (10, 20, 40 nmol/L) were added, respectively, followed by alkaline phosphatase (ALP) staining and the measurement of osteogenesis-related protein expression. RAW264.7 cells were differentiated into macrophages using PMA, and the effects of BMSCs and/or RSPO2 on M1/M2 macrophage polarization were analyzed using qRT-PCR. A rat ACLR model was established, and the rats were divided into four groups: Control, BMSCs, BMSCs+Low RSPO2 (co-injection), and BMSCs+Medium RSPO2 (co-injection). Micro-CT imaging was performed to analyze bone tunnel area and mineralized tissue formation at 4 and 8 weeks post-ACLR. Histological analysis, including HE staining, Safranin O-Fast Green staining, and COL2α1 immunohistochemistry, was used to evaluate tendon-bone healing. Immunofluorescence staining was conducted to detect the expression of M1 (iNOS) and M2 (CD163) macrophage markers at the tendon-bone interface.

Results: RSPO2 significantly promoted the osteogenic differentiation of BMSCs, with the medium concentration of RSPO2 showing the most pronounced effect. RSPO2 and BMSCs also promoted M2 macrophage polarization and inhibited M1 polarization, with the medium concentration of RSPO2 demonstrating the most significant impact. Micro-CT results indicated that RSPO2 and BMSCs treatment significantly reduced the bone tunnel area and increased the formation of mineralized tissue compared to the control group. Histological analysis revealed that RSPO2 and BMSCs treatment improved tendon-bone interface healing, characterized by more orderly fiber tissue arrangement and an increase in chondrocytes and fibrocartilaginous tissue. Immunofluorescence staining results showed that RSPO2 and BMSCs promoted M2 macrophage polarization at the tendon-bone interface.

Conclusions: RSPO2 enhances BMSC-induced osteogenic differentiation and promotes M2 macrophage polarization, thereby improving tendon–bone healing after ACLR surgery in a small-animal model. The combined treatment of RSPO2 and BMSCs demonstrates promising preclinical potential in accelerating bone formation and tendon–bone interface repair, with the medium concentration of RSPO2 showing the most notable effect. However, these findings are based solely on a small-animal model, and further validation in large-animal models and clinical studies is required before potential clinical translation.

Keywords: bone marrow mesenchymal stem cells; R-spondin 2; anterior cruciate ligament reconstruction; tendon-bone

Introduction

Anterior cruciate ligament (ACL) injury, a common sports injury, often leads to severe functional impairment and long-term complications [1,2]. ACL reconstruction surgery is the standard treatment to restore knee joint stability, typically using autografts or allografts [3,4]. However, tendon-bone healing after surgery is limited, resulting in poor functional recovery and an increased risk of postoperative re-injury [5]. The structured reconstruction of the tendon-bone interface and effective bone healing are crucial for the long-term outcome of ACL reconstruction [6,7]. Therefore, exploring novel biomolecules and cellular therapies to promote bone healing has become a key direction in research in this field.

Bone marrow mesenchymal stem cells (BMSCs) have been widely applied in tissue repair and regenerative medicine research due to their excellent osteogenic potential and immunomodulatory effects [8,9]. BMSCs can not only differentiate into osteoblasts but also regulate the local immune environment by secreting various cytokines and signaling molecules, thereby promoting tissue regeneration and wound healing [10]. Studies have shown that BMSCs can induce macrophage polarization into the M2 phenotype during bone healing, creating a favorable environment for repair [11,12]. However, the therapeutic efficacy of BMSCs remains suboptimal, and is influenced by individual differences and local microenvironmental factors in clinical setting. Therefore, identifying molecules that can enhance the efficacy of BMSCs represents a major research focus.

R-spondin 2 (RSPO2), a molecule belonging to the R-spondin family, primarily regulates various biological processes by activating the Wnt/β-catenin signaling pathway and has gained considerable attention in recent years [13–15]. RSPO2 has been shown to have the potential to promote osteoblast proliferation and differentiation in bone tissue, and its role in bone repair is gradually being recognized [16]. A recent study has demonstrated that RSPO2 plays an important role in tendon–bone interface regeneration and ligament insertion healing [17]. Additionally, the potential immunomodulatory role of RSPO2, especially its influence on macrophage polarization, warrants further exploration.

Based on this, the present study aims to investigate the effects of RSPO2 on bone healing after ACL reconstruction by enhancing the osteogenic differentiation and immunoregulatory functions of BMSCs, particularly promoting M2 macrophage polarization. We hypothesize that RSPO2 can amplify the osteogenic and immunomodulatory potential of BMSCs, facilitating bone healing and accelerating the structural reconstruction of the tendon-bone interface. The findings of this study will provide a theoretical foundation for the application of RSPO2 in orthopedic treatments and offer new perspectives for the development of novel combined therapies to promote bone healing in the future.

Materials and Methods

Cell Culture

Mouse BMSCs (iCell-0116a) and RAW264.7 cells (iCell-m047) were purchased from Cellverse Co., Ltd. (Shanghai, China). The cells were cultured in an incubator at 37 °C with 5% CO_2, and maintained in DMEM (PM00031, Proteintech, Wuhan, China) containing 10% FBS (PM00011), 100 U/mL penicillin, and 100 µg/mL streptomycin (PR40022). All cell lines used in this study were authenticated for species identification, and all tested negative for mycoplasma contamination. Mouse BMSCs adhere to plastic culture surfaces and exhibit a spindle-shaped morphology. With increasing passages, the cells become progressively more homogeneous, displaying a whirlpool-like or parallel arrangement with clear cell boundaries and good proliferative capacity.

Osteogenic Differentiation of BMSCs

First, BMSCs were seeded at an appropriate density onto culture plates and cultured in regular medium until the cell density reached 70%–80%. Then, the medium was replaced with osteogenic induction medium containing 10 mM β-glycerophosphate, 50 µg/mL ascorbic acid, and 100 nM dexamethasone. Different concentrations (10, 20, and 40 nmol/L) of human recombinant RSPO2 protein (120-43-20UG, Thermo Fisher Scientific, Waltham, MA, USA) were added to the osteogenic differentiation induction medium, followed by continuous culture for 14 days, with fresh medium replaced every two days. During this period, cell morphology was regularly observed under a microscope, showing gradual elongation of cells and the formation of mineralized nodules as osteogenic differentiation progressed.

ALP Staining

On the 14th day of osteogenic differentiation, the medium was removed, and the cells were washed 2–3 times with PBS. Cells were then fixed with 4% paraformaldehyde for 10 minutes, followed by three additional PBS washes. According to the instructions of the alkaline phosphatase (ALP) staining kit, the staining working solution was prepared and added to the fixed cells. The cells were incubated in the dark at room temperature for 10 minutes, until a blue-purple staining signal appeared. After staining, the cells were rinsed with distilled water to terminate the reaction. The stained cells were then observed and photographed under a light microscope (BX53, Olympus, Tokyo, Japan), where ALP-positive cells showed a blue-purple color. Additionally, the staining results were semi-quantified using image analysis software (version 2.9.0, National Institutes of Health (NIH), Bethesda, MD, USA) to assess the degree of osteogenic differentiation.

Western Blotting

First, the cells or tissue samples were added to RIPA lysis buffer (R0010, Solarbio, Beijing, China) containing protease inhibitors and lysed on ice for 30 minutes. Then, the samples were centrifuged at 12,000 rpm for 10 minutes, and the supernatant was collected as the protein sample. After determining the protein concentration using a BCA kit (PC0020, Solarbio, Beijing, China), the protein samples were mixed with sample buffer and heated at 95 °C for 5 minutes to denature the proteins. Next, the samples were loaded onto an SDS-PAGE gel for electrophoresis and transferred to a PVDF membrane (IPVH00010, Solarbio, Beijing, China) after protein separation. After the transfer, the membrane was blocked with a 5% BSA solution at room temperature for 1 hour, followed by overnight incubation

with the primary antibodies (RUNX2 (1:1000, ab192256, Abcam, Cambridge, UK), COL1 (1:1000, ab316222, Abcam, Cambridge, UK), BMP-2 (1:1000, ab214821, Abcam, Cambridge, UK), OCN (1:1000, ab93876, Abcam, Cambridge, UK), GAPDH (1:1000, ab181602, Abcam, Cambridge, UK)) at 4 °C. The next day, the membrane was washed with TBST and incubated with HRP-conjugated secondary antibodies (1:1000, ab6721, Abcam, Cambridge, UK) at room temperature for 1 hour. After another wash, the membrane was immersed in ECL chemiluminescent reagent for signal detection using a gel imaging system (ChemiDoc MP, Bio-Rad Laboratories, Hercules, CA, USA). Finally, quantitative analysis of the protein bands was performed using ImageJ software (version 2.9.0, NIH, Bethesda, MD, USA), normalizing to GAPDH to assess the relative expression levels of the target proteins.

Macrophage Activation and Culture

First, RAW264.7 cells were seeded into culture dishes and cultured in regular medium until they reached 70%–80% confluence. Then, the cells were treated with 100 nM PMA to induce activation for 24 hours. Meanwhile, BMSCs were seeded into another culture dish and cultured in regular medium until they reached 70%–80% confluence. The BMSCs were treated with different concentrations (10, 20, 40 nmol/L) of RSPO2 recombinant protein for 24 hours. Subsequently, the activated RAW264.7 cells were co-cultured with RSPO2-treated BMSCs in a Transwell system, with RAW264.7 cells placed in the upper chamber and BMSCs in the lower chamber. The co-culture system was incubated at 37 °C with 5% CO_2 for 48 hours.

qRT-PCR

First, total RNA was extracted from cells using an RNA extraction kit (R1200, Solarbio, Beijing, China), and the RNA concentration and purity were measured. Next, the extracted RNA was transcribed into cDNA using a reverse transcription kit (K16215, Solarbio, Beijing, China), with the process carried out at 37 °C using a thermal cycler (Applied Biosystems™ 2720, Thermo Fisher Scientific, Waltham, MA, USA) for 15 minutes. Then, the qRT-PCR reaction mix was prepared, including the cDNA template, specific primers, SYBR Green, qPCR Master Mix, etc., and the reaction mixture was aliquoted into qPCR tubes. The reaction conditions were as follows: initial denaturation at 95 °C for 1 minute, followed by 40 amplification cycles of 95 °C for 5 seconds (denaturation), 60 °C for 30 seconds (annealing/extension), and fluorescence signal collection. After amplification, a melt curve analysis was performed, with a gradual increase in temperature to observe fluorescence signal changes and ensure the specificity of the amplification products. Finally, the Ct values generated by the real-time fluorescence quantitative PCR instrument (QuantStudio 12K Flex, Thermo Fisher Scientific, Waltham, MA, USA) were analyzed, and the relative expression level of the target gene was normalized using an internal reference gene (β-actin), typically calculated using the $2^{-\Delta\Delta Ct}$ method. The primer sequences used in this study are listed in Table 1.

Establishment of ACLR Surgical Model

A total of 48 male Wistar rats (6–7 weeks old, 180 ± 20 g) were purchased from Charles river (Beijing, China). All animals were housed under standard conditions (12-hour light/dark cycle, humidity 40–60%, temperature 23 °C) with free access to food and water. After one week of adaptive feeding, the animals were used for subsequent experiments. First, rats were anesthetized via intraperitoneal injection of sodium pentobarbital (40 mg/kg) to ensure stable body temperature and maintain a sterile environment. A small incision was made on the anterolateral side of the rat's knee joint to expose the joint. Then, microsurgical tools (Beaver™ Mini Blades, Beaver-Visitec International, Waltham, MA, USA) were used to transect the anterior cruciate ligament (ACL) in the ACL region. Throughout the procedure, care was taken to avoid damage to surrounding structures, such as the meniscus and patellar ligament. Following complete ligament transection, the skin and soft tissue were sutured layer by layer, and postoperative analgesia was administered to alleviate pain. During ACL reconstruction surgery, the lateral peroneus longus tendon of the rat ankle was selected as the graft material. A 0.9-mm drill bit (Twist Drill, Dentsply Sirona, York, PA, USA) was used to create bone tunnels on the femur and tibia sides. The graft was fixed with bone screws on the lateral side of the bone tunnels to ensure stability. After the surgery, the soft tissues of the knee joint were repaired, and the wound was sutured layer by layer. Postoperative analgesia was administered to the rats, and appropriate activity restriction was implemented to promote recovery and prevent complications. All rats were randomly divided into four groups: control (12 rats); BMSCs (12 rats); BMSCs + Low RSPO2 (10 nmol/L) (12 rats); BMSCs + Medium RSPO2 (20 nmol/L) (12 rats). The control group received intra-articular injections of 50 µL PBS on the day of surgery, postoperative day 3, and postoperative day 7. In the BMSCs, BMSCs + Low RSPO2, and BMSCs + Medium RSPO2 groups, equivalent volumes of untreated BMSCs (10^5 cells/mL) or BMSCs treated with Low/Medium RSPO2 (10^5 cells/mL) were injected intra-articularly on the same schedule. Before each injection, the rat's knee was flexed to 90° to increase joint space, and the injection was made in the central line of the patellar tendon to avoid damage to intra-articular ligaments. At 6 weeks after treatment, all rats were euthanized by intraperitoneal injection of sodium pentobarbital (180 mg/kg). The tendon–bone interface tissue, bone tunnel region tissue, and knee joint synovial tissue were harvested from each group. The study has been approved by the Beijing Keweite Laboratory Animal Welfare Ethics Committee (approval No. KWT-2023-1223-03).

Table 1. Primer sequences.

Primer name	Primer sequences (5′-3′)
Mus-*ITGAM*-F	CGACACCATCGCATCTAA
Mus-*ITGAM*-R	TCCCTGAACATCACCACC
Mus-*β*-actin-F	GGCTGTATTCCCCTCCATCG
Mus-*β*-actin-R	CCAGTTGGTAACAATGCCATGT
Mus-*CD14*-F	TCTTGAACCTCCGCAACG
Mus-*CD14*-R	CAGCATCCCGCAGTGAAT
Mus-*iNOS*-F	GAGCGAGTTGTGGATTGTC
Mus-*iNOS*-R	CCAGGAAGTAGGTGAGGG
Mus-*IL-6*-F	TGCCTTCTTGGGACTGAT
Mus-*IL-6*-R	CTGGCTTTGTCTTTCTTGTT
Mus-*IL-1β*-F	CTCGTGCTGTCGGACCCAT
Mus-*IL-1β*-R	CAGGCTTGTGCTCTGCTTGTGA
Mus-*TNF-α*-F	GGCGGTGCCTATGTCTCA
Mus-*TNF-α*-R	CCTCCACTTGGTGGTTTGT
Mus-*Arg1*-F	AAGACAGCAGAGGAGGTG
Mus-*Arg1*-R	AGTCAGTCCCTGGCTTAT
Mus-*TGF-β*-F	GGCGGTGCTCGCTTTGTA
Mus-*TGF-β*-R	TCCCGAATGTCTGACGTATTGA
Mus-*CD163*-F	GCCTCTGCTGTCACTAACG
Mus-*CD163*-R	CCACGGACACTTCATTCA
Mus-*IL-10*-F	TTTCAAACAAAGGACCAG
Mus-*IL-10*-R	GGATCATTTCCGATAAGG

Micro-CT Analysis

At 6 weeks after treatment, bone tunnel region tissues were collected from the rats. First, the samples were prepared to be scanned, which typically need to be treated with a fixative to ensure stability during the scanning process. Then, the relevant parameters were set on the Micro-CT device (SkyScan 1275, Bruker, Kontich, Belgium. Resolution: 19.8 µm; Exposure time: 1000 ms; Voltage: 50 kV; Current: 200 µA) to ensure the appropriate position in the scanning region of the sample. Next, during the scanning, the sample was rotated and imaged at different angles through X-rays. After scanning, software was used for image reconstruction, converting the raw X-ray data into two-dimensional or three-dimensional images. Once reconstruction was complete, a Micro-CT analysis software (Bruker microCT software suite, Bruker, Kontich, Belgium) for image post-processing and quantitative analysis was applied. Finally, the analysis results were displayed using virtual slicing or three-dimensional reconstruction images, and statistical analysis was performed to assess the experimental effects.

Hematoxylin-Eosin Staining

At 6 weeks after treatment, tendon–bone interface tissues of the rat knee joint were collected. First, paraffin-embedded tissue sections with a thickness of 5 µm were prepared and placed on glass slides. The sections were deparaffinized using xylene, then hydrated with a gradient of ethanol, followed by rinsing with distilled water. Next, the sections were immersed in hematoxylin solution for 5 minutes, rinsed until the cell nuclei appeared blue-violet, and differentiated with 1% hydrochloric acid ethanol to restore the blue color. Then, the sections were immersed in eosin solution for 3 minutes to stain the cytoplasm pink. Afterward, the sections were dehydrated with a gradient of ethanol, cleared with xylene, and finally mounted the slides with a mounting medium and allowed to dry. The stained sections were observed and photographed under a microscope, and quantitative analysis was performed using Image J software (version 1.53t, National Institutes of Health, Bethesda, MD, USA).

Orange Red O-Green Solid Staining

At 6 weeks after treatment, tendon–bone interface tissues of the rat knee joint were collected. First, 5 µm thick paraffin-embedded tissue sections were prepared and performed dewaxing and hydrated. The paraffin was removed using xylene, followed by stepwise hydration with ethanol of different concentrations, and finally rinsed with distilled water. Next, the sections were immersed in Orange Red O solution for 10 minutes. After staining, the sections were rinsed with distilled water and then immersed in Green Solid solution for 5 minutes. Subsequently, the sections were rinsed with distilled water and performed dehydration using ethanol and xylene stepwise for transparency. Finally, a mounting medium was used to mount the sections and allowed to dry. The stained sections were observed under a microscope, with the cytoplasm appearing orange-

red and collagen fibers appearing green, which helps distinguish tissue components. Quantitative analysis was performed using ImageJ software (version 1.53t, National Institutes of Health, Bethesda, MD, USA).

Immunohistochemistry (IHC)

At 6 weeks after treatment, tendon–bone interface tissues of the rat knee joint were collected. First, the tissue sections were deparaffinized and hydrated, followed by antigen retrieval using heat. Then, the sections were blocked with blocking solution to prevent nonspecific binding. The primary antibody (Collagen II) (1:1000, AF5456, Affinity, Liyang, China) was added and incubated overnight at 4 °C. Afterward, the sections were washed to remove unbound antibodies, and the HRP-labeled secondary antibody (1:1000, ab6721, Abcam, Cambridge, UK) was added and incubated for 1 hour at room temperature. Next, DAB chromogenic solution was used to visualize the target protein, which would appear brown. Hematoxylin counterstaining may be optionally performed. After completion, the sections were dehydrated, cleared, and mounted with mounting medium. Finally, the stained sections were observed under a microscope (BX53, Olympus, Tokyo, Japan) and the expression of the target protein was evaluated.

Immunofluorescence Staining

At 6 weeks after treatment, knee joint synovial tissues were collected from the rats. First, the samples were fixed with 4% paraformaldehyde for 10 minutes, then washed with PBS and permeabilized with 0.1% Triton X-100 for 5 minutes, followed by another PBS wash. Next, the samples were blocked with 5% BSA for 30–60 minutes to reduce nonspecific binding. The specific primary antibodies (CD163 (1:1000, ab182422, Abcam, Cambridge, UK), iNOS (1:1000, ab178945, Abcam, Cambridge, UK)) were added and incubated overnight at 4 °C or for 1 hour at room temperature. After washing with PBS, the Alexa Fluor 594-labeled secondary antibody (1:1000, ab150080, Abcam, Cambridge, UK) was added and incubated in the dark at room temperature for 1 hour, followed by another PBS wash. Optionally, the nuclei were stained with DAPI, then washed with PBS. Anti-fade mounting medium was added, covered with a coverslip, and finally, the fluorescence signal of proteins in the samples was observed under a fluorescence microscope (Axio Imager, Carl Zeiss AG, Oberkochen, Germany) and their expression and localization were analyzed. Quantitative analysis of protein expression was performed using Image J software (version 1.53t, National Institutes of Health, Bethesda, MD, USA).

Statistical Analysis

Data were analyzed using GraphPad Prism software (version 9.0, GraphPad Software, Inc., San Diego, CA, USA), with statistical significance defined as $p < 0.05$. Differences between the two groups were compared using *t*-tests, while one-way ANOVA followed by Tukey's post-hoc test was applied for comparisons across multiple groups.

Results

RSPO2 Promotes Osteogenic Differentiation of BMSCs

Low, medium, and high concentrations of RSPO2 recombinant protein (10, 20, 30 nmol/L) were added during the osteogenic induction culture of BMSCs, respectively. After 7 days of culture, BMSCs were subjected to ALP staining, with results shown in Fig. 1a,b. Compared to the control group, treatment with RSPO2 at high, medium, and low concentrations significantly increased the ALP staining intensity of BMSCs ($p < 0.05$). Compared to the low-concentration RSPO2 treatment group, the medium-concentration RSPO2 treatment group showed a significant increase in ALP staining intensity ($p < 0.05$). However, compared to the medium-concentration RSPO2 treatment group, the high-concentration treatment group exhibited a significant decrease in ALP staining intensity ($p < 0.05$). We also measured the expression levels of osteogenic-related proteins in BMSCs. Results shown in Fig. 1c–g indicate that the protein expression levels of RUNX2, COL1, BMP-2, and OCN were significantly higher in the RSPO2 treatment groups at all concentrations compared to the control group ($p < 0.05$). Compared to the low-concentration RSPO2 treatment group, the medium-concentration treatment group showed a significant increase in the protein expression levels of RUNX2, COL1, BMP-2, and OCN ($p < 0.05$). In contrast, the high-concentration RSPO2 treatment group showed significantly lower protein expression levels of RUNX2, COL1, BMP-2, and OCN compared to the medium-concentration treatment group ($p < 0.05$). These results suggest that the promoting effect of RSPO2 on osteogenic differentiation of BMSCs is not dose-dependent and only the optimal dose produces the maximum promoting effect.

BMSCs and/or RSPO2 Synergistically Promote M2 Polarization of Macrophages

We used PMA (100 nM) to stimulate RAW264.7 cells for macrophage differentiation for 48 hours. The mRNA levels of macrophage markers CD14 and CD11b in RAW264.7 cells were measured. The results in Fig. 2a,b show that, compared to the PBS group, the mRNA levels of CD11b and CD14 were significantly increased in the PMA group. This indicates that RAW264.7 cells were successfully induced into macrophages. To investigate the potential effects of RSPO2 and BMSCs on macrophages, we treated macrophages with RSPO2 and/or BMSCs. The results in Fig. 2c–f show that, compared to the control group, the mRNA expression of M1 macrophage markers (iNOS,

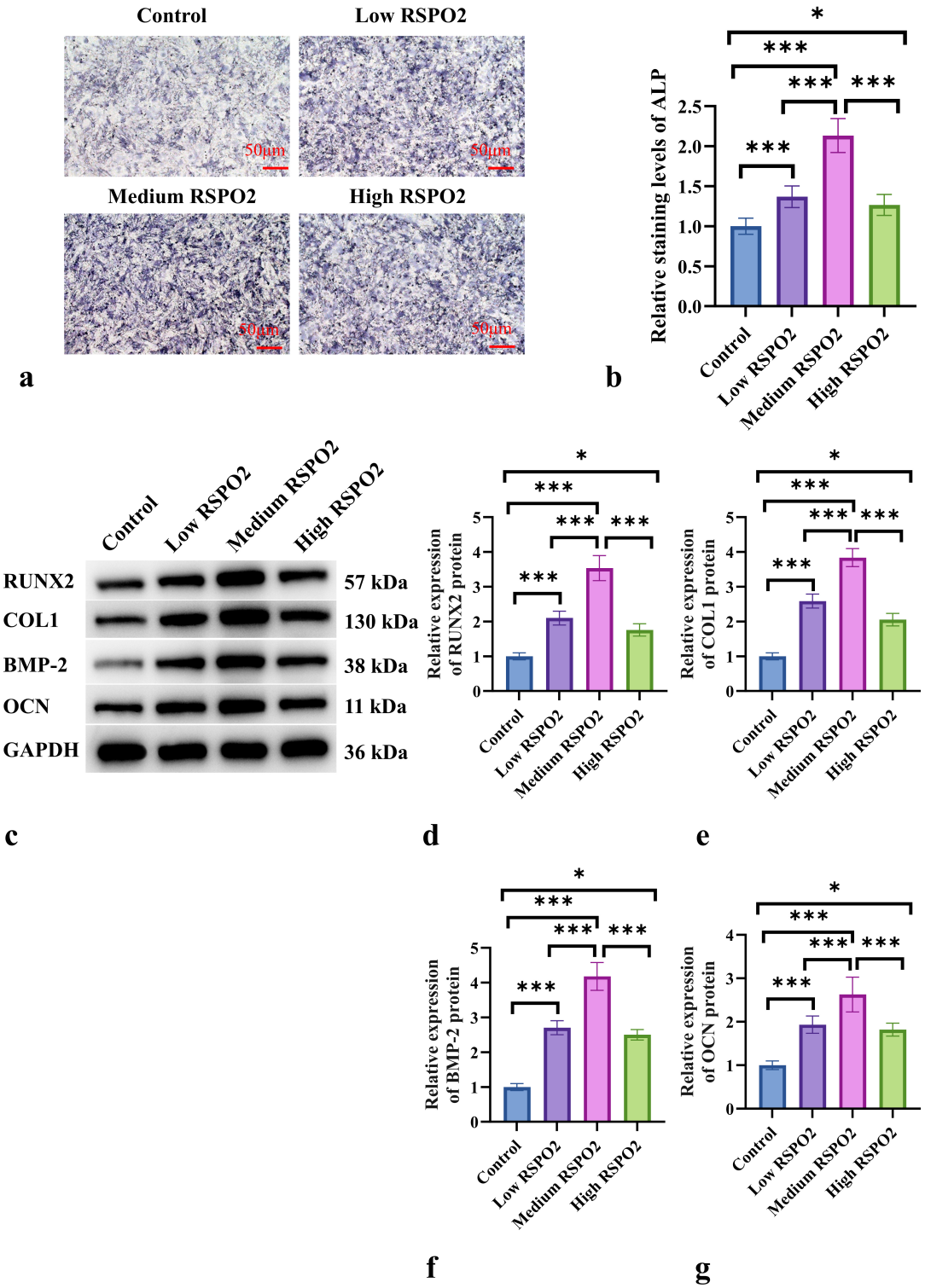

Fig. 1. RSPO2 promotes osteogenic differentiation of BMSCs. (a,b) ALP staining results of BMSCs induced for osteogenic differentiation for 14 days under different concentrations of RSPO2 treatment. (c–g) Expression of osteogenic-related proteins RUNX2, COL1, BMP-2, and OCN in BMSCs induced for osteogenic differentiation for 14 days. n = 6. *$p < 0.05$, ***$p < 0.001$. RSPO2, R-spondin 2; BMSCs, bone marrow–derived mesenchymal stem cells; ALP, alkaline phosphatase.

IL-6, IL-1β, and TNF-α) was significantly reduced in the BMSCs group ($p < 0.05$). Compared to the BMSCs-only treatment group, the mRNA expression levels of iNOS, IL-6, IL-1β, and TNF-α were significantly lower in the BMSCs+Low RSPO2 and BMSCs+Medium RSPO2 groups ($p < 0.05$), with the reduction being more significant in the

BMSCs+Medium RSPO2 group ($p < 0.05$). The results in Fig. 2g–j revealed that, compared to the control group, the mRNA expression of M2 macrophage markers (CD163, IL-10, TGF-β, and Arg-1) was significantly increased in the BMSCs group ($p < 0.05$). Compared to the BMSCs-only treatment group, the mRNA expression levels of CD163, IL-10, TGF-β, and Arg-1 were significantly increased in the BMSCs+Low RSPO2 and BMSCs+Medium RSPO2 groups ($p < 0.05$), with the increase being more significant in the BMSCs+Medium RSPO2 group ($p < 0.05$). These results suggest that RSPO2 accelerates the polarization of macrophages toward M2 by BMSCs.

Micro-CT Imaging Analysis of ACLR After BMSCs and/or RSPO2 Treatment

Micro-CT was used to analyze the area of the femoral and tibial tunnel on the joint surface at 6 weeks post-surgery (Fig. 3a). For the tunnel regions, at 6 weeks post-surgery, the tunnel areas on both femoral and tibial sides in the BMSCs, BMSCs+Low RSPO2, and BMSCs+Medium RSPO2 groups were significantly smaller than in the control group ($p < 0.05$), with the BMSCs+RSPO2 treatment groups showing significantly smaller tunnel areas compared to the BMSCs-only group ($p < 0.05$), and the Medium RSPO2 group exhibiting the smallest tunnel areas ($p < 0.05$) (Fig. 3b,c). We also measured the formation of mineralized tissue in the tunnel's scaffold (BV/TV). The results in Fig. 3d,e show that at 6 weeks post-surgery, the BV/TV values in the BMSCs, BMSCs+Low RSPO2, and BMSCs+Medium RSPO2 groups were significantly increased compared to the control group ($p < 0.05$). Compared to the BMSCs-only treatment group, the BV/TV values in the BMSCs+Low RSPO2 and BMSCs+Medium RSPO2 groups more significantly increased ($p < 0.05$), with the BV/TV values on the femoral and tibial sides being significantly higher in the BMSCs+Medium RSPO2 group compared to the BMSCs+Low RSPO2 group ($p < 0.05$). In summary, the combined treatment of BMSCs and RSPO2 results in more mineralized tissue formation in the bone tunnels on both femoral and tibial sides, with the best therapeutic effect observed in the BMSCs+Medium RSPO2 group.

Histological Analysis After ACLR Surgery

Finally, we observed the histological changes in the tissues after anterior cruciate ligament reconstruction (ACLR) surgery. HE staining results (Fig. 4a,b) showed that at 6 weeks, the BMSCs+Low RSPO2 and BMSCs+Medium RSPO2 groups displayed more orderly fibrovascular tissue. Additionally, compared to the control group, the BMSCs, BMSCs+Low RSPO2, and BMSCs+Medium RSPO2 groups showed a significant reduction in the relative width of the bone-graft interface at 6 weeks, with the relative width being notably shorter than that of the control group ($p < 0.05$).

Next, we performed Picro-Sirius Red-Olive Green staining to observe chondrocytes and fibrocartilage at the tendon-bone interface. Our results (Fig. 4c,d) showed that BMSCs and/or RSPO2 treatment significantly increased the number of chondrocytes and fibrocartilage at the tendon-bone interface. Compared to the BMSCs group, the BMSCs+Low RSPO2 group significantly increased chondrocytes and fibrocartilage at the tendon-bone interface ($p < 0.05$). Furthermore, compared to the BMSCs+Low RSPO2 group, the BMSCs+Medium RSPO2 group exhibited even more chondrocytes and fibrocartilage formation ($p < 0.05$).

To quantify collagen fiber remodeling, the expression of COL2α1 protein was detected using IHC. As shown in Fig. 4e,f, compared to the control group, COL2α1 positive staining was significantly increased in the BMSCs group at 6 weeks ($p < 0.05$). In comparison to the BMSCs group, the BMSCs+Low RSPO2 and BMSCs+Medium RSPO2 groups also showed significant increases in COL2α1 positive staining at 6 weeks, with the staining intensity in the latter being significantly stronger than in the former ($p < 0.05$).

BMSCs and/or RSPO2 Treatment Promotes M2 Macrophage Polarization at the Tendon-Bone Healing Interface

IF staining was performed to measure the expression of M1 macrophage marker (iNOS) and M2 macrophage marker (CD163) at the tendon-bone interface tissue 6 weeks after ACLR surgery. The results in Fig. 5a–d show that compared to the control group, BMSCs treatment significantly increased the positive expression of CD163 ($p < 0.05$) and decreased the positive expression of iNOS ($p < 0.05$). Compared to the BMSCs group, the BMSCs+Low RSPO2 and BMSCs+Medium RSPO2 groups showed a significant increase in the positive expression of CD163 ($p < 0.05$) and a reduction in the positive expression of iNOS ($p < 0.05$). Additionally, the BMSCs+Medium RSPO2 group exhibited a significantly higher level of positive CD163 expression ($p < 0.05$) and a significant reduction in iNOS positive expression ($p < 0.05$) compared to the BMSCs+Low RSPO2 group.

Discussion

This study demonstrates that RSPO2 accelerates bone healing after ACL reconstruction by enhancing the osteogenic differentiation of BMSCs and promoting M2 macrophage polarization. Our findings are consistent with previous studies and provide new insights into the potential role of RSPO2 in bone repair.

We observed that RSPO2 significantly enhanced the osteogenic differentiation of BMSCs, as evidenced by increased alkaline phosphatase (ALP) activity and upregulation of osteogenic markers, such as RUNX2, COL1, BMP-2, and OCN. Interestingly, the effect of RSPO2 on osteo-

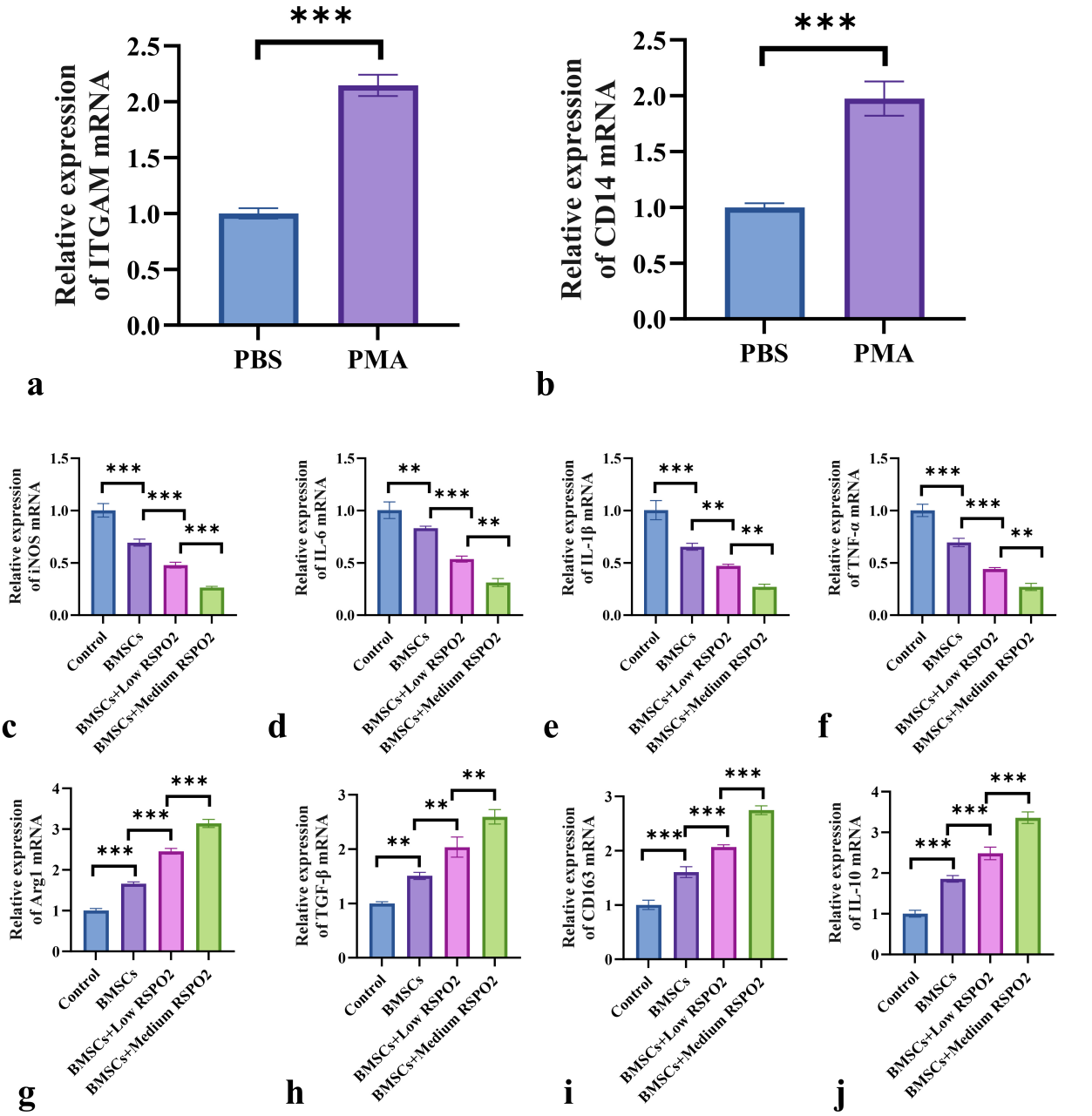

Fig. 2. BMSCs and/or RSPO2 synergistically promote M2 polarization of macrophages. (a,b) RAW264.7 cells were stimulated with PMA for 24 hours, and the expression levels of *ITGAM* and CD14 were measured to verify whether RAW264.7 cells were successfully activated into macrophages. (c–f) qRT-PCR was used to measure the mRNA expression of M1 macrophage markers (iNOS, IL-6, IL-1β, TNF-α) in macrophages. (g–j) qRT-PCR was used to measure the mRNA expression of M2 macrophage markers (Arg1, TGF-β, CD163, IL-10) in macrophages. n = 6. $^{**}p < 0.01$, $^{***}p < 0.001$.

genesis was not dose-dependent, with moderate concentrations showing the most significant effect. This is consistent with the findings of Mai Arima *et al.* [18], who also reported that RSPO2 promotes osteoblast differentiation through the Wnt/β-catenin pathway. However, in our study, high concentrations of RSPO2 appeared to inhibit osteogenic activity above a certain threshold, suggesting that further research is needed to optimize the treatment dosage.

We investigated the role of RSPO2 in macrophage polarization and found that when used in combination with BMSCs, RSPO2 promoted M2 macrophage polarization and reduced the expression of M1 markers. Consistent with the findings reported by Wang *et al.* [19], that BMSCs promote tissue repair by inducing M2 polarization, our study further confirms these findings and demonstrates that RSPO2 enhances the polarization. This suggests that RSPO2 not only boosts the osteogenic potential of BMSCs

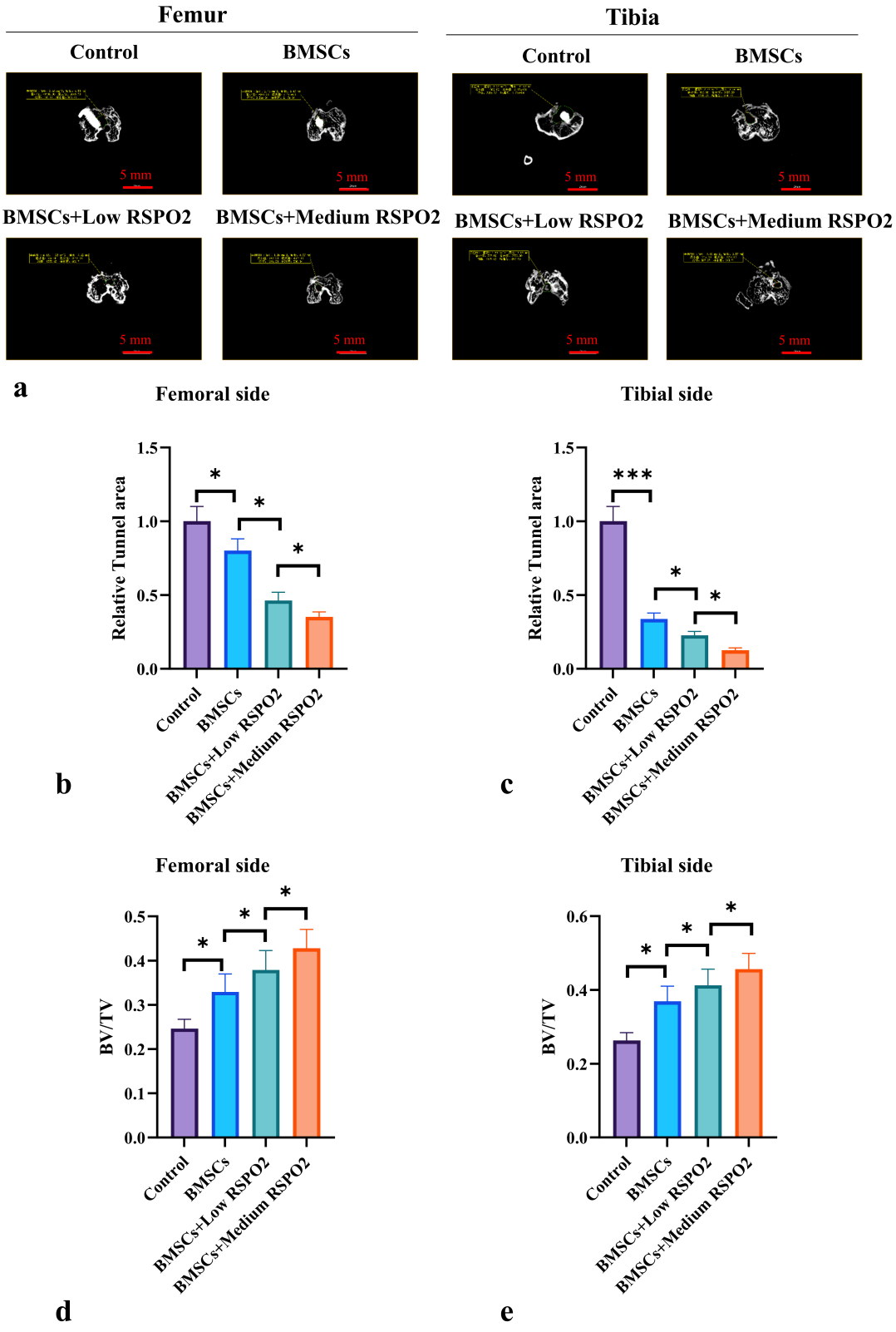

Fig. 3. Micro-CT Imaging Analysis of ACLR After BMSCs and/or RSPO2 Treatment. (a) Cross-sectional Micro-CT images of bone tunnels on the femoral and tibial sides. (b,c) Relative tunnel areas on the femoral and tibial sides at 6 weeks after ACLR surgery. (d,e) Bone volume/total volume ratio (BV/TV) on the femoral and tibial sides at 6 weeks after ACLR surgery. n = 6, *$p < 0.05$, ***$p < 0.001$. ACLR, anterior cruciate ligament reconstruction.

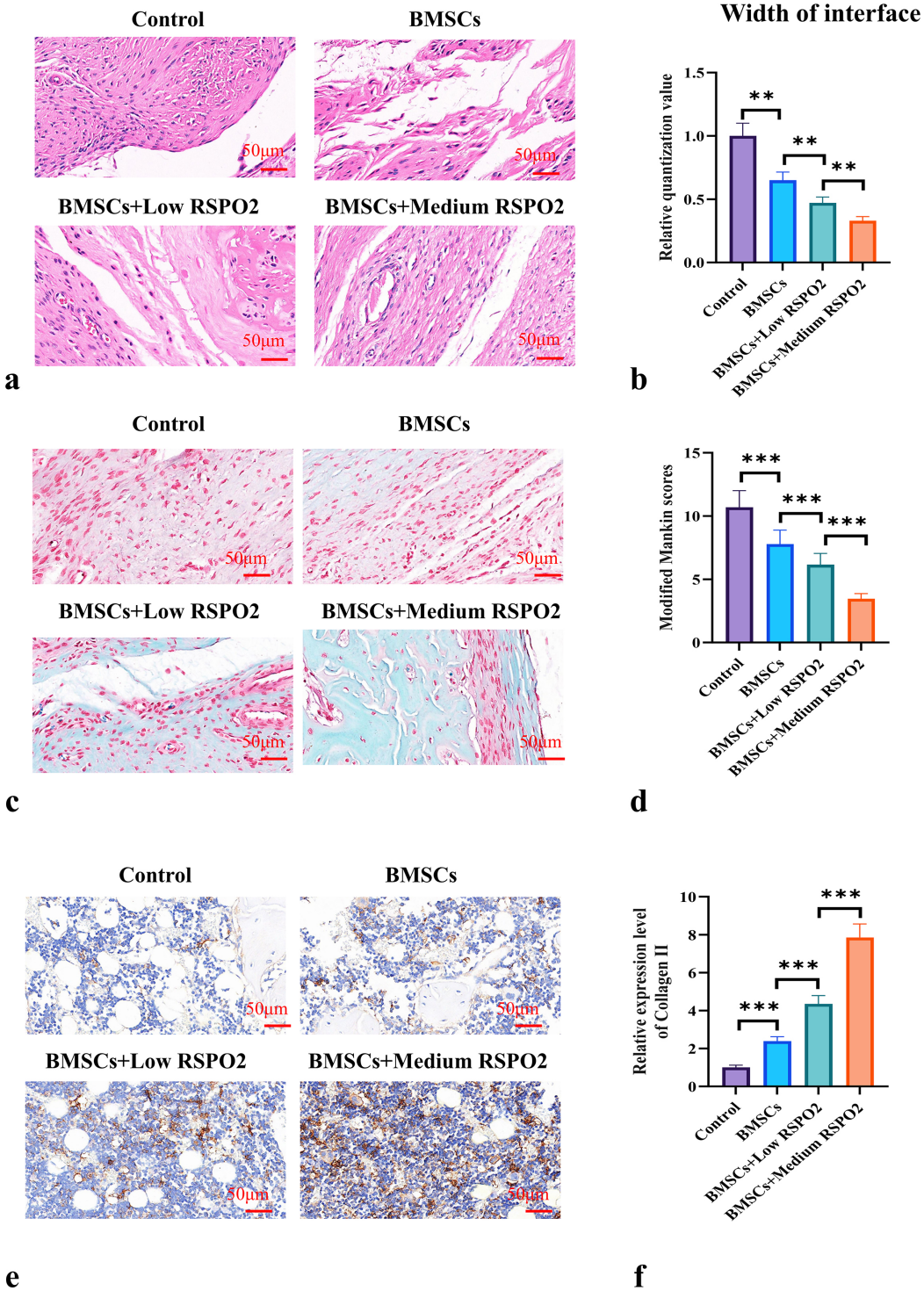

Fig. 4. Histological Analysis After ACLR Surgery. (a,b) Representative images of the tendon-bone interface at 6 weeks after ACLR surgery with different treatments through HE staining, and quantification of the relative width of the interface. (c,d) Picro-Sirius Red-Olive Green staining at the tendon-bone interface at 6 weeks after ACLR surgery, with quantitative analysis of fibrocartilage. (e,f) Immunohistochemical detection of COL2α1 expression at the tendon-bone interface at 6 weeks after ACLR surgery. n = 6, $^{**}p < 0.01$, $^{***}p < 0.001$.

but also creates a favorable immunoregulatory microenvironment that may accelerate bone healing. The specific molecular mechanisms by which RSPO2 regulates immune cell behavior warrant further investigation.

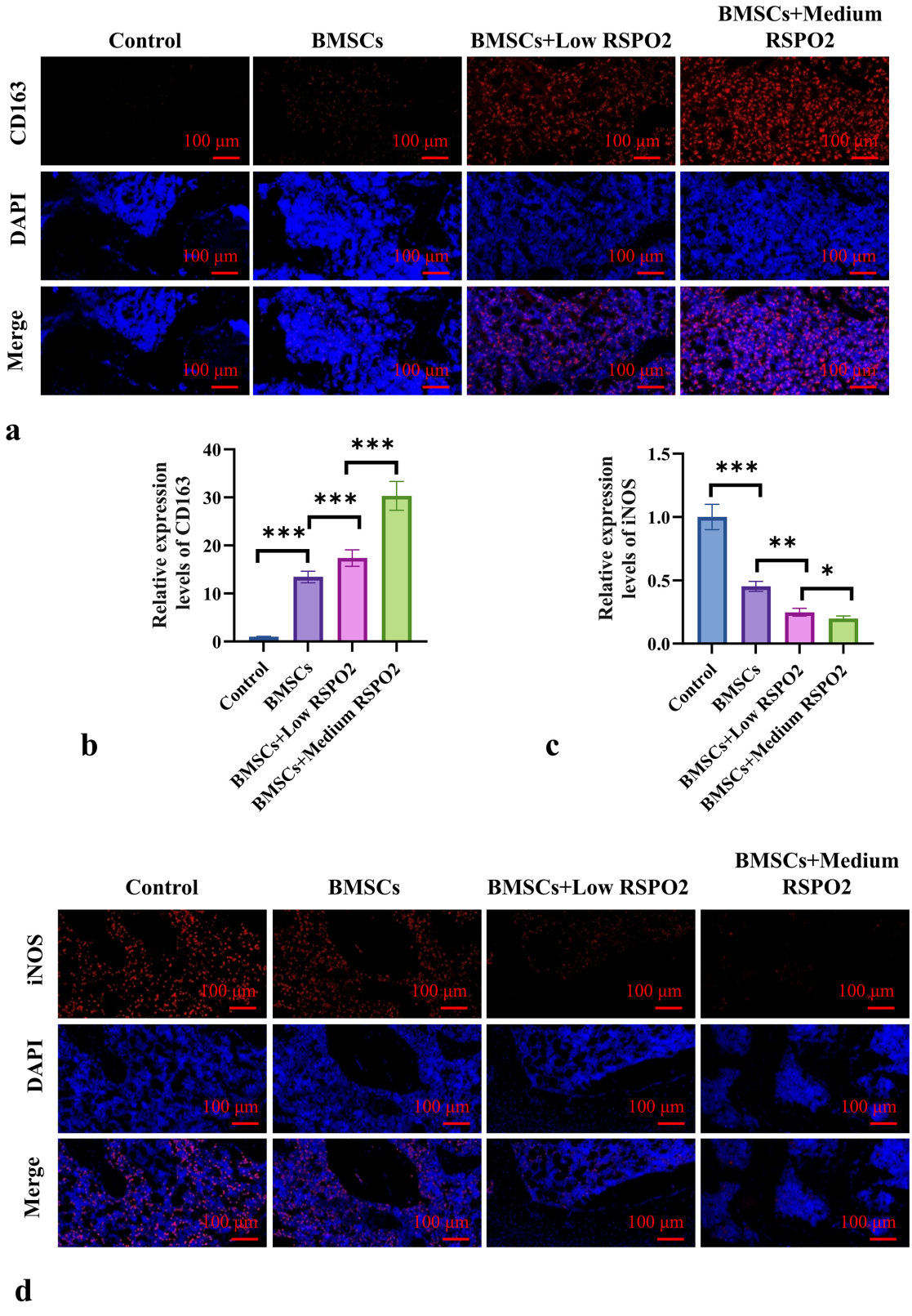

Fig. 5. BMSCs and/or RSPO2 Treatment Promotes M2 Macrophage Polarization at the Tendon-Bone Healing Interface. (a,b) Expression of CD163 at the tendon-bone interface 6 weeks after ACLR surgery measured by immunofluorescence staining. (c,d) Expression of iNOS at the tendon-bone interface 4 weeks after ACLR surgery measured by immunofluorescence staining. n = 6. *$p < 0.05$, **$p < 0.01$, ***$p < 0.001$.

Through Micro-CT analysis, we confirmed that the bone tunnel area was smaller and the bone volume fraction (BV/TV) increased in the RSPO2 treatment group, with the most significant effect observed at moderate concentrations. This finding is consistent with the study by Nora Alhazmi *et al*. [20], who demonstrated the role of RSPO2 in promoting bone regeneration in a cranial defect model. Our research provides new insights into the effectiveness of RSPO2 in the ACL reconstruction model, which differs from traditional bone defect models in its mechanical environment. This difference highlights the potential broad applicability of RSPO2 in promoting bone healing across different tissue contexts.

Histological analysis further confirmed the role of RSPO2 in promoting tendon-bone healing. We observed that the fibrous structure at the tendon-bone interface was more organized in the RSPO2 treatment group, with increased formation of cartilage and fibrocartilage, particularly at moderate concentrations. These findings are consistent with the study by Gao *et al*. [21], who highlighted the importance of fibrocartilage formation in tendon-bone connection. RSPO2 may enhance this process by creating a healing environment that favors fibrocartilage formation and structural remodeling.

Immunofluorescence analysis showed that RSPO2 treatment increased the expression of the M2 macrophage marker CD163 at the tendon-bone interface and decreased the expression of the M1 marker iNOS. This finding is consistent with the report by Wang *et al*. [22], who indicated that M2 macrophages play a key role in tissue repair. By demonstrating that RSPO2 amplifies BMSC-induced M2 polarization, we propose its potential synergistic effect in improving healing outcomes through immune modulation.

Based on our current experimental findings, we propose that RSPO2 regulates macrophage polarization through both direct and indirect BMSC-mediated mechanisms. First, our *in vitro* macrophage experiments demonstrated that RSPO2 alone was able to shift macrophage polarization toward an M2 phenotype, as evidenced by increased expression of M2-associated markers and suppression of M1-associated markers. This suggests that RSPO2 can act directly on macrophages, potentially through activation of Wnt/β-catenin–related signaling pathways, which have been reported to influence macrophage phenotype regulation. Second, RSPO2 markedly enhanced the osteogenic differentiation capacity of BMSCs and amplified the immunomodulatory function of BMSCs, leading to a stronger pro-regenerative microenvironment. BMSCs are known to secrete paracrine factors that influence macrophage behavior, and RSPO2 stimulation likely augments this effect, thereby indirectly promoting M2 polarization via BMSC–macrophage crosstalk. Therefore, we hypothesize that RSPO2 exerts a dual regulatory role in the tendon–bone healing process after ACL reconstruction: (1) direct modulation of macrophage polarization, and (2) indirect enhancement of BMSC-mediated immunoregulation and osteogenesis.

Despite the significant potential of our findings, there are several limitations in this study. First, our research primarily focused on the early stages of bone healing and did not evaluate the long-term effects of RSPO2 treatment on bone quality and functional recovery. Future studies should include extended observation periods to assess the persistence and quality of newly formed bone. Additionally, although we demonstrated the role of RSPO2 in promoting M2 macrophage polarization, its underlying molecular mechanisms remain unclear. Future research should explore how RSPO2 interacts with specific signaling pathways, such as the Wnt/β-catenin pathway, and immune-related pathways that regulate macrophage polarization and osteogenesis.

Another limitation is the use of a rat ACL reconstruction model, which may not fully replicate the complexity of human ACL injury and bone healing. While animal models offer valuable insights, clinical translation will require further validation in larger animal models and, ultimately, confirmation through human trials. Although local RSPO2 administration promoted osteogenesis and tendon–bone healing in a rat ACLR model, the potential risk of ectopic ossification associated with intra-articular RSPO2 delivery cannot be excluded, particularly in human knees. Previous research suggests that RSPO2 may interact with inflammatory pathways, including NF-κB–related signaling, which has been implicated in pathological osteogenesis and heterotopic ossification under inflammatory conditions [16].

It should be noted that no ectopic bone formation was observed in this study. However, the applicability of these findings may be constrained by a small-animal model and a limited observation period, which might not fully capture delayed or uncommon adverse effects. Future studies in large-animal models with longer follow-up and controlled RSPO2 dosing are required to further evaluate safety and translational feasibility. Moreover, only male rats were used in this study. Given that sex hormones, particularly estrogen, can influence macrophage polarization and immune responses, this design choice may limit the generalizability of our findings to females [23]. Consequently, future studies incorporating female animals are needed to assess potential sex-specific effects.

In addition, although the results from imaging, histological, and immunological analyses suggested improved tendon–bone healing, the absence of biomechanical testing (e.g., graft pull-out strength testing) represents a key limitation. Therefore, the functional relevance of the observed structural improvements requires further validation through mechanical assessment in subsequent research.

Future research should focus on several key directions. First, exploring the long-term effects of RSPO2 on bone quality and functional recovery is crucial for understanding its full therapeutic potential, including evaluating

whether RSPO2 can reduce reinjury rates or improve the long-term effects of tendon-bone integration. Second, determining the optimal dosage of RSPO2 for bone healing is important, as our results suggest that excessively high concentrations may inhibit osteogenesis. Future studies should aim to identify the best treatment window. Additionally, investigating the molecular mechanisms behind RSPO2's dual role in osteogenesis and immune modulation could help develop more targeted therapies. Understanding how RSPO2 interacts with specific immune cell subpopulations and signaling pathways may pave the way for combination therapies that promote bone regeneration and regulate immunity. Finally, clinical studies are essential for translating these preclinical findings into human applications. RSPO2 holds significant therapeutic potential for promoting bone healing across a spectrum of orthopedic conditions, including ACL injuries, fractures, and other tendon-bone integration issues.

Conclusions

In conclusion, this study provides strong evidence that RSPO2 accelerates bone healing after ACL reconstruction by enhancing the osteogenic differentiation of BMSCs and promoting M2 macrophage polarization. These findings highlight RSPO2 as a potential therapeutic target for improving clinical outcomes in bone and tendon healing. Future research should focus on optimizing the dosage of RSPO2, understanding its molecular mechanisms, and validating its efficacy in clinical settings.

Availability of Data and Materials

The data that support the findings of this study are available from the corresponding author upon reasonable request.

Author Contributions

CBW and YY designed the research study. CBW performed the research. CBW provided help and advice on the experiments. YY analyzed the data. CBW drafted the manuscript. Both authors contributed to important editorial changes in the manuscript. Both authors read and approved the final manuscript. Both authors have participated sufficiently in the work and agreed to be accountable for all aspects of the work.

Ethics Approval and Consent to Participate

The study has been approved by the Beijing Keweite Laboratory Animal Welfare Ethics Committee (approval No. KWT-2023-1223-03).

Acknowledgment

Not applicable.

Funding

This research received no external funding.

Conflict of Interest

The authors declare no conflict of interest.

References

[1] van Melick N, van der Weegen W, van der Horst N, Bogie R. Double-Leg and Single-Leg Jump Test Reference Values for Athletes With and Without Anterior Cruciate Ligament Reconstruction Who Play Popular Pivoting Sports, Including Soccer and Basketball: A Scoping Review. The Journal of Orthopaedic and Sports Physical Therapy. 2024; 54: 377–390. https://doi.org/10.2519/jospt.2024.12374.

[2] Gwathmey FW. Precision Anterior Cruciate Ligament Reconstruction. Clinics in Sports Medicine. 2024; 43: xiii–xiv. https://doi.org/10.1016/j.csm.2024.02.002.

[3] Ebert JR, Calvert ND, Radic R. A Prospective Randomized Controlled Trial Investigating Quadriceps Versus Hamstring Tendon Autograft in Anterior Cruciate Ligament Reconstruction. The American Journal of Sports Medicine. 2024; 52: 660–669. https://doi.org/10.1177/03635465231222279.

[4] Xerogeanes J. Editorial Commentary: Quadriceps Tendon Is a Better Graft Than Hamstring for Anterior Cruciate Ligament Reconstruction. Arthroscopy: The Journal of Arthroscopic & Related Surgery: Official Publication of the Arthroscopy Association of North America and the International Arthroscopy Association. 2024; 40: 1245–1246. https://doi.org/10.1016/j.arthro.2023.09.028.

[5] Shen S, Lin Y, Sun J, Liu Y, Chen Y, Lu J. A New Tissue Engineering Strategy to Promote Tendon-bone Healing: Regulation of Osteogenic and Chondrogenic Differentiation of Tendon-derived Stem Cells. Orthopaedic Surgery. 2024; 16: 2311–2325. https://doi.org/10.1111/os.14152.

[6] Yu C, Chen R, Chen J, Wang T, Wang Y, Zhang X, *et al*. Enhancing tendon-bone integration and healing with advanced multi-layer nanofiber-reinforced 3D scaffolds for acellular tendon complexes. Materials Today. Bio. 2024; 26: 101099. https://doi.org/10.1016/j.mtbio.2024.101099.

[7] Simon-Sanchez FJ, Perelli S, Pizza N, Delmedico M, Morales-Avalos R, Torres Claramunt R, *et al*. Short and proximalized interference screw fixation leads to tibial tunnel bone re-growth and better hamstring graft integration in ACL reconstruction. Knee Surgery, Sports Traumatology, Arthroscopy: Official Journal of the ESSKA. 2025; 33: 3080–3087. https://doi.org/10.1002/ksa.12551.

[8] Yi G, Zhang R, Li M, Song X, Li S. Atractylenolide-III attenuates osteoarthritis by repolarizing macrophages through inactivating TLR4/NF-κB signaling. International Immunopharmacology. 2024; 129: 111629. https://doi.org/10.1016/j.intimp.2024.111629.

[9] Wang K, Peng X, Zhang R, Wu X, Mao L. COL6A3 enhances the osteogenic differentiation potential of BMSCs by promoting mitophagy in the osteoporotic microenvironment. Molecular Biology Reports. 2024; 51: 206. https://doi.org/10.1007/s11033-023-08918-z.

[10] Liu J, Li F, Ouyang Y, Su Z, Chen D, Liang Z, *et al*. Naringin-

induced M2 macrophage polarization facilitates osteogenesis of BMSCs and improves cranial bone defect healing in rat. Archives of Biochemistry and Biophysics. 2024; 753: 109890. https://doi.org/10.1016/j.abb.2024.109890.

[11] Zhu D, Peng T, Zhang Z, Guo S, Su Y, Zhang K, *et al*. Mesenchymal stem cells overexpressing XIST induce macrophage M2 polarization and improve neural stem cell homeostatic microenvironment, alleviating spinal cord injury. Journal of Tissue Engineering. 2024; 15: 20417314231219280. https://doi.org/10.1177/20417314231219280.

[12] Chen X, Wan Z, Yang L, Song S, Fu Z, Tang K, *et al*. Exosomes derived from reparative M2-like macrophages prevent bone loss in murine periodontitis models via IL-10 mRNA. Journal of Nanobiotechnology. 2022; 20: 110. https://doi.org/10.1186/s12951-022-01314-y.

[13] Gong Y, Yuan S, Sun J, Wang Y, Liu S, Guo R, *et al*. R-Spondin 2 Induces Odontogenic Differentiation of Dental Pulp Stem/Progenitor Cells via Regulation of Wnt/β-Catenin Signaling. Frontiers in Physiology. 2020; 11: 918. https://doi.org/10.3389/fphys.2020.00918.

[14] Tachibana N, Chijimatsu R, Okada H, Oichi T, Taniguchi Y, Maenohara Y, *et al*. RSPO2 defines a distinct undifferentiated progenitor in the tendon/ligament and suppresses ectopic ossification. Science Advances. 2022; 8: eabn2138. https://doi.org/10.1126/sciadv.abn2138.

[15] Niehrs C, Seidl C, Lee H. An “R-spondin code” for multimodal signaling ON-OFF states. BioEssays: News and Reviews in Molecular, Cellular and Developmental Biology. 2024; 46: e2400144. https://doi.org/10.1002/bies.202400144.

[16] Liu F, Zhao Y, Pei Y, Lian F, Lin H. Role of the NF-kB signalling pathway in heterotopic ossification: Biological and therapeutic significance. Cell Communication and Signaling: CCS. 2024; 22: 159. https://doi.org/10.1186/s12964-024-01533-w.

[17] Nakajima M, Kou I, Ohashi H, Genetic Study Group of the Investigation Committee on the Ossification of Spinal Ligaments, Ikegawa S. Identification and Functional Characterization of RSPO2 as a Susceptibility Gene for Ossification of the Posterior Longitudinal Ligament of the Spine. American Journal of Human Genetics. 2016; 99: 202–207. https://doi.org/10.1016/j.ajhg.2016.05.018.

[18] Arima M, Hasegawa D, Yoshida S, Mitarai H, Tomokiyo A, Hamano S, *et al*. R-spondin 2 promotes osteoblastic differentiation of immature human periodontal ligament cells through the Wnt/β-catenin signaling pathway. Journal of Periodontal Research. 2019; 54: 143–153. https://doi.org/10.1111/jre.12611.

[19] Wang Y, Wang J, Gao R, Liu X, Feng Z, Zhang C, *et al*. Biomimetic glycopeptide hydrogel coated PCL/nHA scaffold for enhanced cranial bone regeneration via macrophage M2 polarization-induced osteo-immunomodulation. Biomaterials. 2022; 285: 121538. https://doi.org/10.1016/j.biomaterials.2022.121538.

[20] Alhazmi N, Carroll SH, Kawasaki K, Woronowicz KC, Hallett SA, Macias Trevino C, *et al*. Synergistic roles of Wnt modulators R-spondin2 and R-spondin3 in craniofacial morphogenesis and dental development. Scientific Reports. 2021; 11: 5871. https://doi.org/10.1038/s41598-021-85415-y.

[21] Gao S, Hu C, Wang Y, Zhang J, Tang K. Comparison of cortical versus cancellous bone fixation in tendon-to-bone healing with a rat trans-calcaneal suture model for Achilles tendon sleeve avulsion. Journal of Orthopaedic Surgery and Research. 2023; 18: 15. https://doi.org/10.1186/s13018-022-03469-8.

[22] Wang H, Yu H, Huang T, Wang B, Xiang L. Hippo-YAP/TAZ signaling in osteogenesis and macrophage polarization: Therapeutic implications in bone defect repair. Genes & Diseases. 2023; 10: 2528–2539. https://doi.org/10.1016/j.gendis.2022.12.012.

[23] Enright S, Werstuck GH. Investigating the Effects of Sex Hormones on Macrophage Polarization. International Journal of Molecular Sciences. 2024; 25: 951. https://doi.org/10.3390/ijms25020951.